Sensors and Actuators B 243 (2017) 29–35

Contents lists available at ScienceDirect

Sensors and Actuators B: Chemical

journal homepage: www.elsevier.com/locate/snb

# Self-assembly biomimetic fern leaf-like $\alpha$-$Fe_2O_3$ for sensing inflammable 1-butanol gas

Hong Pan, Long Jin, Binbin Zhang, Hai Su, Haitao Zhang, Weiqing Yang*

*Key Laboratory of Advanced Technologies of Materials (Ministry of Education), School of Materials Science and Engineering, Southwest Jiaotong University, Chengdu 610031, China*

ARTICLE INFO

*Article history:*
Received 19 August 2016
Received in revised form
13 November 2016
Accepted 16 November 2016
Available online 24 November 2016

*Keywords:*
$\alpha$-$Fe_2O_3$
Fern leaf-like structure
1-butanol
Gas sensors

ABSTRACT

Self-assembly biomimetic fern leaf-like $\alpha$-$Fe_2O_3$ (SABFF) has been synthesized by a facile template-free hydrothermal process. The SEM images of this sample evidently reveal that the crystal nucleus with hexagonal structure is self-assembly sculptured and gradually grows the regular six biomimetic fern leaf-like $\alpha$-$Fe_2O_3$ along six corners. Furthermore, the stem of the individual fern leaf-like $\alpha$-$Fe_2O_3$ with the length of approximately 6 μm and the width of 9–12 nm was clearly demonstrated in the TEM images. Based on it, we developed a ceramic tube gas sensor, presenting the high-performance sensitivity of 2 ppm for inflammable 1-butanol gas. Also, this gas sensor exhibits excellent selectivity and stability. The corresponding response and recovery times of 100 ppm 1-butanol were optimized to be about 34 s and 21 s, respectively. Therefore, this kind of SABFF will be a potential excellent gas sensing materials for safety monitor in an explosive or inflammable atmosphere.



## 1. Introduction

Due to increasingly worsening environmental pollution issues, gas sensors based on micro/nanomaterials have gained considerable interest owing to their applications in environmental monitoring, air-quality control, and detection of inflammable, explosives and toxic gases [1–4]. It is well known that high sensitivity, rapid response, and excellent selectivity are three most important parameters in designing gas sensors. Therefore, the demand for both the sensors and the sensing materials to meet the real-time monitoring requirements for a variety of applications, has accelerated the development of new sensing materials and sensors technology.

Hematite $\alpha$-$Fe_2O_3$ with a wide band gap of 2.1 eV, a typical *n*-type semiconductor, is the most stable iron oxide in ambient conditions. It has been extensive applied in catalysts, gas sensors, optical devices, water splitting, lithium-ion batteries and magnetic devices [5–12], owing to its high resistance to corrosion, low cost, biocompatible, environmentally friendly and non-toxic. Up to now, various $\alpha$-$Fe_2O_3$ structures such as 0 D nanoparticles [13], 1 D nanowires [14], nanorods [11], or nanotubes [7], 2D plates or sheets [15], 3D spheres [5,16,17] and flower- or urchin-like structures [6,18,19], have been successfully prepared by various methods and applied in many fields.

Previous researches about $\alpha$-$Fe_2O_3$-based sensors were investigated on the detection of $C_2H_5OH$, diethylamine, $H_2S$, and acetone [7,19–21]. However, the $\alpha$-$Fe_2O_3$-based gas sensor to detect 1-butanol has rarely been reported. 1-butanol is a volatile and stimulating liquid, which is wildly used as solvent, organic synthesis intermediates and extracting agent. People may suffer a serious injury, when exposed to 1-butanol environment, causing an irritation to the respiratory system and skin. Moreover, as a kind of alcohols, volatile and flammable 1-butanol can cause an explosion in the state of gas, when mixed with air. Thus, it is imperatively necessary to design high sensitivity and selectivity sensors to detect 1-butanol for the safety in production and environmental protection.

In this work, we reported a facile template-free hydrothermal method to synthesize SBFF by adjusting the pH value. Based on it, this developed gas sensor exhibited high-performance sensitivity of 2 ppm inflammable 1-butanol gas, excellent stability and selectivity among some gases such as alcohols, methanol, ethanol, and 1-butanol. Evidently, this kind of SABFF-based 1-butanol gas sensors would open up a way for safety monitor in an explosive or inflammable atmosphere.

* Corresponding author.
*E-mail address:* wqyang@swjtu.edu.cn (W. Yang).

http://dx.doi.org/10.1016/j.snb.2016.11.080
0925-4005/

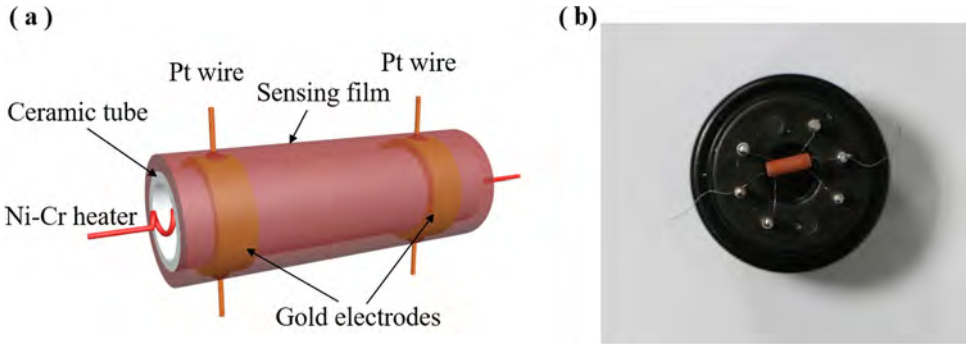


**Fig. 1.** The (a) schematic structure and (b) photography images of the $\alpha$-$Fe_2O_3$ gas sensors.

## 2. Experimental section

### 2.1. Material

All the reagents in the experiment were of analytical grade and used without further purification.

### 2.2. Synthesis process

The $\alpha$-$Fe_2O_3$ was prepared according to the reported method with some modification [22]. Briefly, 0.3 g $K_3Fe(CN)_6$ was dispersed in 70 ml distilled water to form a suspension solution, adjusting the pH value to 8.0 with 0.1 M ammonia solution. The solution was then transferred into a 100 ml Teflon-lined stainless steel autoclave. After sealing, the autoclave was heated at 150 °C for 48 h, and then cooled naturally. The production was collected by centrifugation, washed with deionized water and absolute ethanol several times, and finally dried in vacuum at 60 °C. The red products of $\alpha$-$Fe_2O_3$ were obtained.

### 2.3. Characterization

The size and morphology of the reaction products were characterized by X-ray powder diffraction, which was carried out on an X'PertPro X-ray diffractometer (XRD, X'PertPro, Philips, Netherlands). The main parameters are as follows: the X-ray generator was operated at 40 kV and 40 mA by applying Cu $K_\alpha$ radiation. Data sets were collected within the range of 20–80 ° with the scanning rate of 0.02 ° per second. Scanning electron microscopy (SEM, S4800) images of $\alpha$-$Fe_2O_3$ were also taken. Transmission electron microscopy (TEM, JEOL-2100-f, JEOL, Japan) and HRTEM operating at an accelerating voltage of 120 and 200 kV, respectively. As-prepared samples were ultrasonic dispersed by ethanol. Then the suspension of composites were dropped on the copper grids and dried in air.

### 2.4. Fabrication and measurement of gas sensor

The products were mixed with moderate amounts of deionized water to form a paste. Then the paste were coated on a ceramic tube form a sensing layer. A pair of Au electrodes was installed at each end of the ceramic tube before it was coated with the paste, and each electrode was connected with two Pt wires. Finally, a heating wire (Ni-Cr alloy) was put in the center of the ceramic tube to form an indirect-heated gas sensor [23]. The schematic structure and photography images of the $\alpha$-$Fe_2O_3$ gas sensor is shown in Fig. 1.

The electrical properties of the sensor were measured on a WS-30A system (Weisheng Instruments Co., Zhengzhou, China) and determined under laboratory conditions (32 ± 1 RH%, 15 ± 2 °C). During this experiment the constant measurement voltage is 5 V.

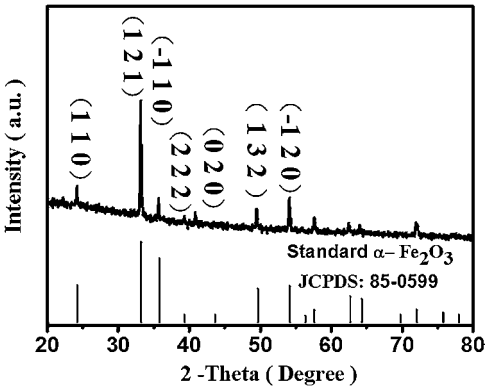


**Fig. 2.** XRD patterns and standard card (JCPDS: 85-0599) of the fern leaf like $\alpha$-$Fe_2O_3$.

The response is defined as $S = R_a/R_g$ ($R_a$ and $R_g$ are the resistance for sensors in air and in target gas, respectively). The operating temperature is ranging from 220 to 300 °C. The response and recovery times taken by the resistor reaching to 90% of finial equilibrium value was defined as the response time ($\tau_{res}$) in the case of adsorption or the recovery time ($\tau_{recov}$) in the case of desorption.

## 3. Results and discussion

### 3.1. Structural and morphological characteristics

The XRD pattern of SABFF is shown in Fig. 2. It is obvious that all of the observed peak positions are in good consistent with the hexagonal structure of the standard card of $\alpha$-$Fe_2O_3$ (JCPDS No. 85-0599). The $\alpha$-$Fe_2O_3$ products peaks are relatively sharp in intensity, indirectly certifying that the obtained products by hydrothermal reaction at 150 °C for 48 h have ordinary crystallinity. Furthermore, no impurities diffraction peaks from any other impurities are observed in the XRD pattern, indicating the excellent purity of the products.

To further reveal the self-assembly process mechanism of SBFF, controlling the role reaction time is employed for the insight of morphology into the evolution process of SABFF at the fixed temperature of 150 °C. The corresponding results are shown in Fig. 3. At the early stage (2 h), it can be seen that the crystal nucleus with hexagonal structure formed (Fig. 3a). After the reaction time of 4 h, this crystal nucleus are self-assembly sculptured and gradually grow the regular six biomimetic fern leaf-like $\alpha$-$Fe_2O_3$ along six corners (Fig. 3b). As the reaction proceeded for 6 h, the size of snowflake become larger and the snowflake-like product partly disintegrated (Fig. 3c). Further increasing the reaction time to 24 h, the snowflake-like product nearly disintegrate and the uniform fern leaf-like products have been obtained (Fig. 3d). The morphologies and structures of the synthesized ABSFF are illuminated by

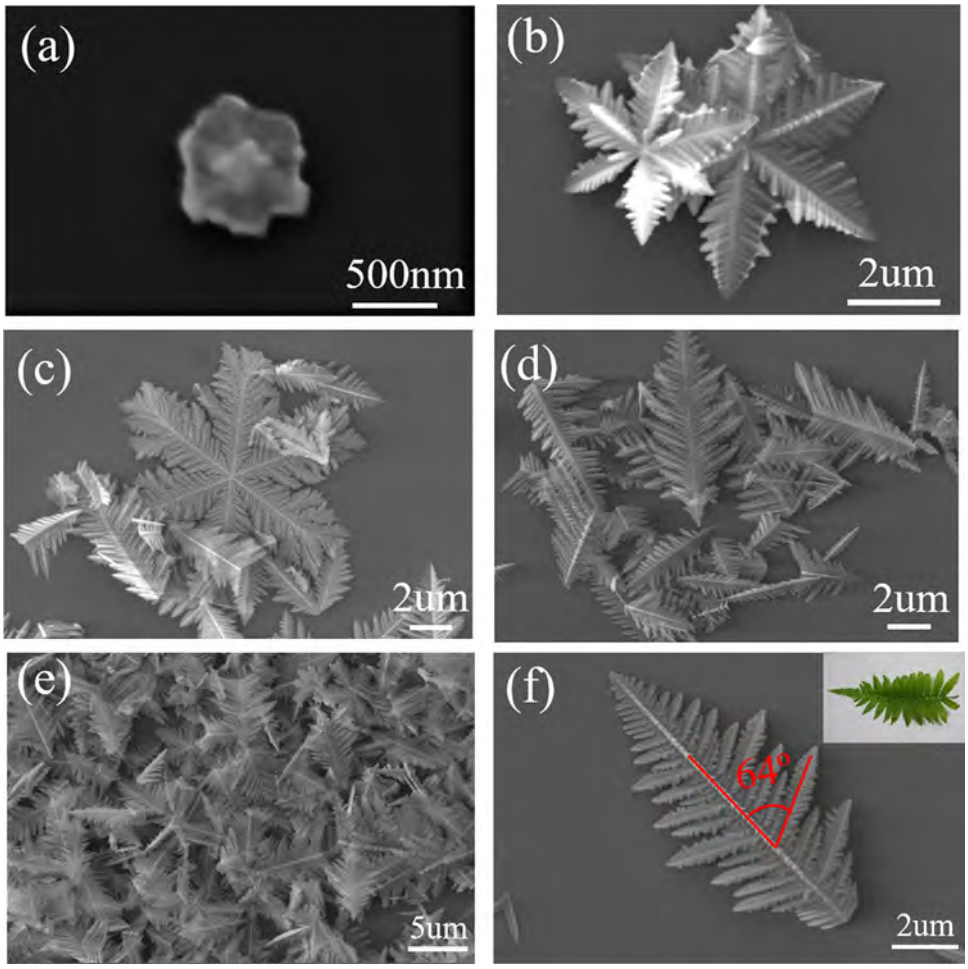


**Fig. 3.** Series of SEM images of the as-prepared products at 150 °C with different time: (a) 2 h, (b) 4 h, (c) 6 h, (d) 24 h (low magnification (e) and high magnification (f)) .The inset is a picture of natural fern leaf.

**Fig. 4.** Schematic illustration of the evolution process of SABFF.

SEM images in Fig. 3e, showing that a typical sample is composed of numerous uniform and independent fern leaf-like $\alpha$-$Fe_2O_3$. As shown in Fig. 3f, this typical fern leaf-like structure is presented in the magnified SEM image, obviously demonstrating that each fern leaf-like structure is constituted of a stem with two groups of highly symmetric and parallel branch. It is extremely similar to a natural fern leaf as shown in inset of Fig. 3f, and the angle between the branch and the main stem was measured to be about 64°. Furthermore, the possible schematic illustration of the evolution process (from Fig. 3a to b) of SABFF is shown in Fig. 4.

The more detailed structural information of the $\alpha$-$Fe_2O_3$ crystals is provided by TEM images. From Fig. 5a–d, it can be observed that the stem is approximately 6 μm in length and 9–12 nm in the width. In addition, HRTEM images are chosen from the stem and branch (Fig. 5d) by a yellow square with different numbers inside (Fig. 4e, f). Fig. 5e (spot 1, Fig. 5d) and Fig. 4f (spot 2, Fig. 5d) show the lattice fringe spacing values of stem and branch are 0.27 and 0.25 nm, which are indexed to the (104) and (110) plane of $\alpha$-$Fe_2O_3$ materials.

In Fig. 6, we can clearly see that $N_2$ adsorption/desorption isotherms is non-porous type, and the BET (Brunauer-Emmett-Teller) surface area of the fern leaf-like alfa-$Fe_2O_3$ is 5.8245 $m^2/g$. Thus, the high sensitivity toward different gas species, is contributed to the fern leaf-like structure in nature, which is highly close to natural leaves. This leaf-like micro-/nanostructure (especially fern leaf-like) was revealed to possess an improved ability for diffusion and adsorption/desorption [24].

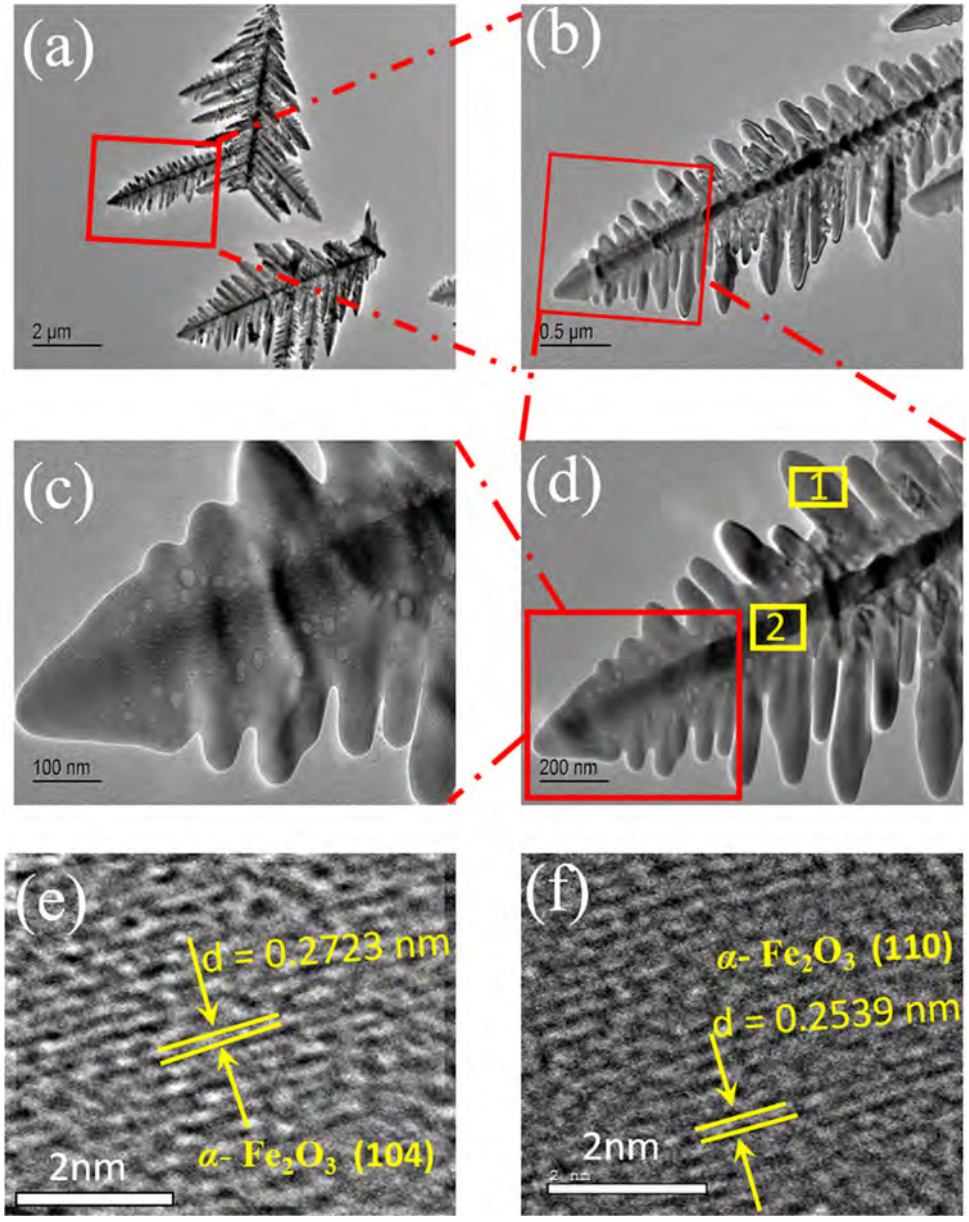


**Fig. 5.** (a–d) The low and high magnification TEM images of fern leaf-like $\alpha$-$Fe_2O_3$, (e–f) HRTEM images taken from spots 1 and 2 in Figure d, respectively.

### 3.2. Gas sensing properties

The operating temperature is an important parameter for semiconductor oxide sensors due to its great influence on the contact reactions between sensing materials and targeting gas. Therefore, parallel experiments were implemented at the range of 220–300 °C to obtain an optimum operating temperature of sensor. The responses of the sensor to 100 ppm 1-butanol at a series of operating temperature are illustrated in Fig. 6. Evidently, the sensitivity of the sensor firstly increases with operating temperature and reaches a maximum value of $S = 8.26$ at the operating temperature of 260 °C, but the responses then decrease with further increase at operating temperature. This decreasing sensitivity at higher temperatures may be ascribed to decreasing in the number of active sites for 1-butanol adsorption [25]. The other possibility is that the rate of desorption is higher than that of adsorption at such high temperature [26–28]. Obviously, the optimum operating temperature for the sensor was evidently proved to be 260 °C, applied in the following investigations.

Fig. 7a shows the dynamic 1-butanol sensing curve of sensor based on the fern leaf-like $\alpha$-$Fe_2O_3$ at 260 °C with the concentration in the range from 2 to 50 ppm, showing reproducible and reversible sensing behaviors. From Fig. 7a, it can be distinctively observed that the response of the sensor presents a ladder-type improvement as the concentration of 1-butanol increases. The corresponding sensitivities are about $S = 1.55, 2.21, 2.90, 3.55$, and 5.24, for the inflammable 1-butanol gas concentration of 2, 5, 10, 20, and 50 ppm, respectively. The specific growth trend of the sensor at 260 °C to high concentration of 1-butanol is displayed in Fig. 7b. The sensing response of the sensor quickly increases in the 1-butanol concentration of below 100 ppm, but its sensitivity at the concentration of over 500 ppm is increasingly relaxed. Namely, the sensitivity of the sensor gradually reaches to the saturation. One possibility is that the sensing response of the sensor highly depends on the removal of oxygen ions via reaction with the target gas. [29,30] As the concentration of the target gas increases, the number of oxygen ions on the surface of the sensing materials will be much less than the quantity of gases. Then, surface reaction

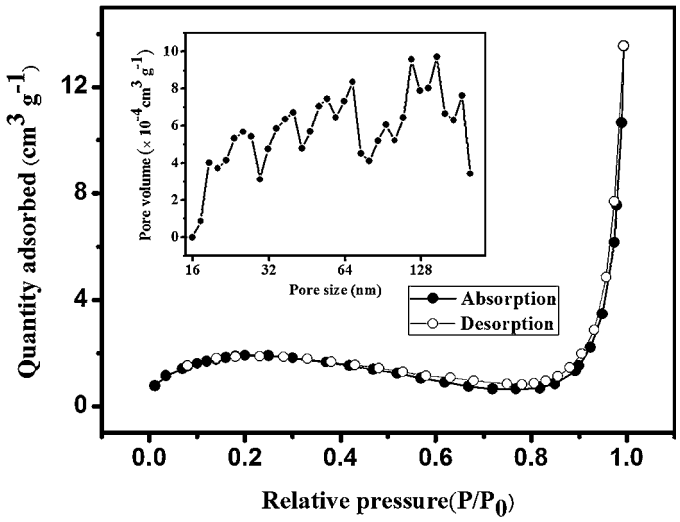


**Fig. 6.** $N_2$ adsorption/desorption isotherms and pore size distribution plot (inset) of fern leaf-like $\alpha$-$Fe_2O_3$.

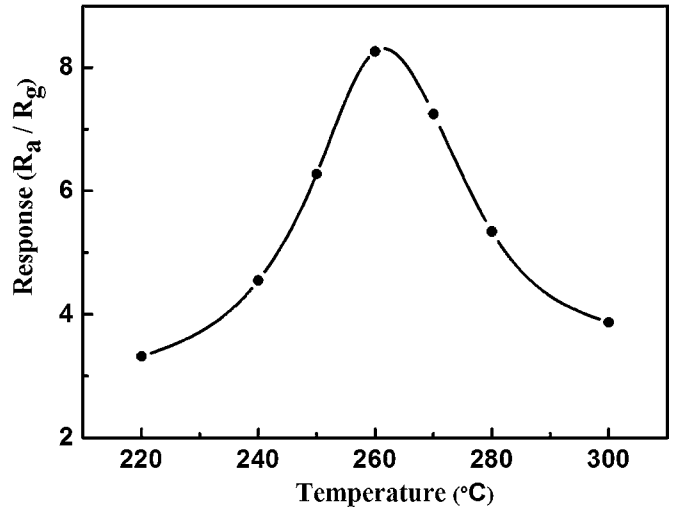


**Fig. 7.** Response of gas sensor as a function of the working temperature to 100 ppm 1-butanol.

**Table 1**
Comparison of the response/recovery time of $\alpha$-$Fe_2O_3$ and $\alpha$-$Fe_2O_3$ compound sensors toward 100 ppm of the 1-butanol.

| sample | Concentration (ppm) | Response Time(s) | Recovery Time(s) |
|---|---|---|---|
| $\alpha$-$Fe_2O_3$ nanorods [31] | 100 | 62 | >25 |
| ZnO-decorated $\alpha$-$Fe_2O_3$ Nanorods [31] | 100 | 55 | 26 |
| $\alpha$-$Fe_2O_3$-ZnO-Au [32] | 100 | >40 | >25 |
| $\alpha$-$Fe_2O_3$-Au [32] | 100 | >40 | 30 |
| This work | 100 | 34 | 21 |

that occurred will be lower, resulting the slow increase speed of the response. The inset in Fig. 7b shows a magnified response of the sensor at the concentration of from 2 ppm to 50 ppm.

The response and the recovery time play a vital role for real-time detection of the toxic gases in the field of gas sensors. Fig. 8a shows that the response and (recovery) times of the sensor based on ABSFF for the 1-butanol concentration of 10, 20, 50, and 100 ppm are 17.5 (9), 24 (16), 26 (18), and 34 s (21s), respectively. It is the fastest value reported in literature for $\alpha$-$Fe_2O_3$ and $\alpha$-$Fe_2O_3$ compound sensors (Table 1) [31,32]. The fast response/recovery time (34s/21 s for 100 ppm 1-butanol) is attributed to the fern leaf-like structure in

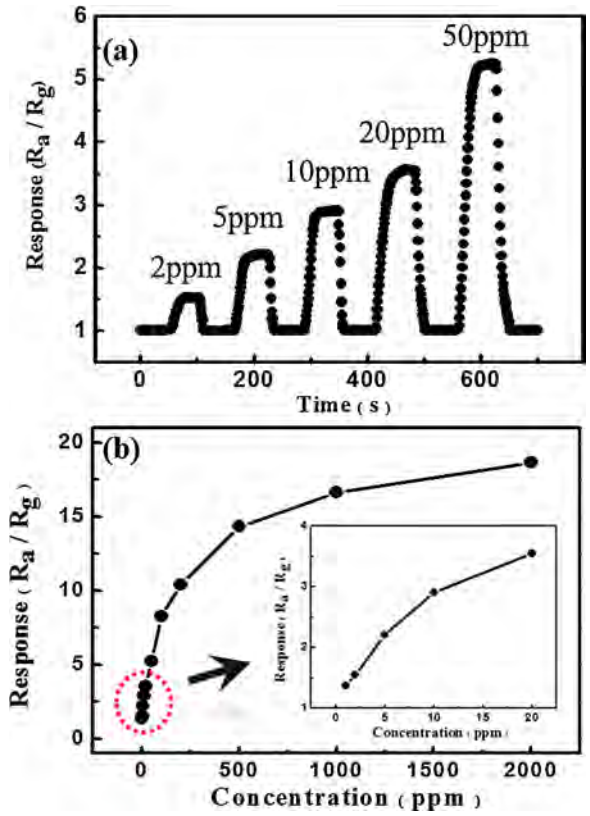


**Fig. 8.** (a) Dynamic sensing response of the fern leaf-like $\alpha$-$Fe_2O_3$ to 2–50 ppm of 1-butanol. (b) The sensing response of the fern leaf-like $\alpha$-$Fe_2O_3$ to 2–2000 ppm of 1-butanol at 260 °C (inset was the response of the sensor to 2–50 ppm 1-butanol).

nature which highly enhance diffusion and adsorption/desorption abilities [25]. In order to further investigate the application value of the obtained sensor, Fig. 8b depicts the selectivity properties of the as-fabricated sensor at the operating temperature of 260 °C for various combustible or toxic gases with the concentration of 100 ppm, such as benzene, toluene, ammonia, methanol, ethanol, and 1-butanol. It can be obviously seen high sensing response to 1-butanol and less sensitive to other gases, indicating that the ABSFF-based gas sensor has a quite good selectivity toward 1-butanol. As the results of experiment on methanol, ethanol and 1-butanol demonstrate, the sensor response will enhancing with the length of alkyl-chain increasing, implying that the length of alkyl-chain has a great effect on the sensor responses [33,34].

For the practical application of the gas sensors, we further investigate the robustness of the as-fabricated sensor. Fig. 9 shows the excellent stability of this sensor during the 1-butanol concentration of 20, 50, 100 ppm at the operating temperature of 260 °C. It can be easily seen that all of the 1-butanol-sensing sensitivity only decreased about 5% as time increased from 1 to 15 days. Thus, the ABSFF-based sensors display an excellent long-term stability.

### 3.3. Gas sensing mechanism

Combined with the above experimental results, the ABSFF-based sensors exhibit excellent gas-sensing properties. For the sensing mechanism of $\alpha$-$Fe_2O_3$ sensors, same as the traditional semiconductor oxide gas sensors [35,36], the most widely accepted theory is based on the change in resistance of the sensor by the adsorption and desorption process of oxygen molecules on the surface of sensing materials. When the sensor was exposed to air,

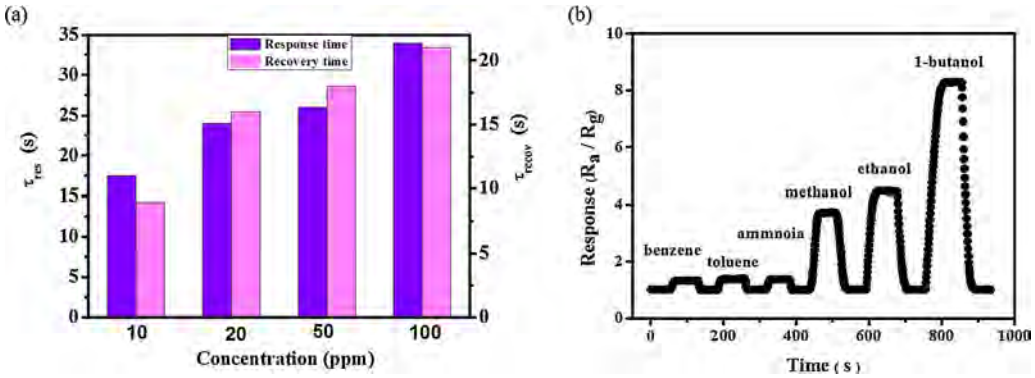


**Fig. 9.** (a) Response/recovery time of the sensor to 10–100 ppm 1-butanol at 260 °C and (b) dynamic sensing response of the sensors to 100 ppm various targeting gases at 260 °C.

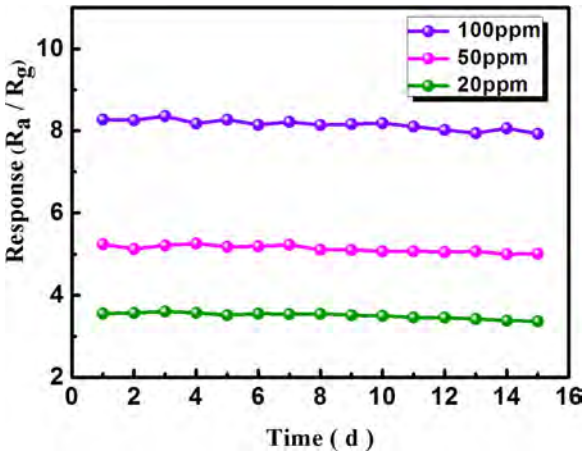


**Fig. 10.** Long-term stabilities of the fern leaf-like $\alpha$-$Fe_2O_3$ sensor to 20, 50, and 100 ppm of 1-butanol at 260 °C, respectively.

oxygen molecules are absorbed onto the fern leaf-like $\alpha$-$Fe_2O_3$ surface, forming oxygen ions ($O^-$, $O_2^-$, $O^{2-}$) [31,32,37].

$$O_2(gas) \rightarrow O_2(ads)$$

$$O_2(ads) + e^- \rightarrow O_2^-(ads)$$

$$O_2^-(ads) + e^- \rightarrow 2O^-(ads)$$

$$O^-(ads) + e^- \rightarrow O^{2-}(ads) \quad (1)$$

Electron depletion layers are formed on the sample surface, increasing the sensor resistance after the chemisorption process reaches equilibrium. When the sensor was exposed to 1-butanol, the 1-butanol gas is oxidized by the oxygen species on the surface, generating water and carbon, as shown in Fig. 10. This process decreases the oxygen ions concentration on the surface and increases the electron concentration, ultimately decreasing the resistance of the sensor. Then, the sample breaks away from the surface 1-butanol gas and restores to its original state in air (Fig. 11).

## 4. Conclusions

In summary, the biomimetic fern leaf-like $\alpha$-$Fe_2O_3$, which is highly close to the natural leaves, has been synthesized by a facile hydrothermal method without any template, catalyst, or substrate. The SEM and TEM images are applied for deep insight into the growth process of unique biomimetic fern leaf-like structure. Importantly, the as-obtained fern leaf-like $\alpha$-$Fe_2O_3$ sensor exhibits fast response/recovery times (34s/21s) to 100 ppm 1-butanol compared to $\alpha$-$Fe_2O_3$ compound sensors. It is contributed to the biomimetic fern leaf-like structure which is extremely significant for gas diffusion and adsorption/desorption. Moreover, the sensor shows good sensitivity, excellent selectivity and stability for inflammable 1-butanol. Thus, this kind of SABFF will be a good potential candidate for high-performance gas sensor for the inflammable and explosive gas monitoring.

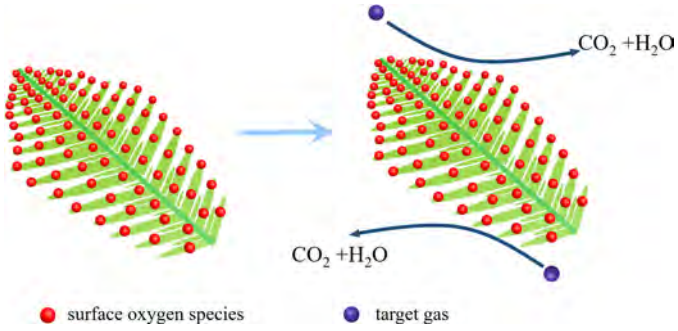


**Fig. 11.** Schematic diagrams on the gas-sensing mechanism of the SABFF.

## Acknowledgements

This work is supported by the scientific and technological projects for Distinguished Young Scholars of Sichuan Province (No.2015JQ0013), the Fundamental Research Funds for the Central Universities of China (A0920502051619-72).

## References

[1] A. Gurlo, Nanosensors: towards morphological control of gas sensing activity. $SnO_2$, $In_2O_3$, ZnO and $WO_3$ case studies, Nanoscale 3 (2011) 154–165.
[2] P.C. Chen, S. Sukcharoenchoke, K. Ryu, L.G. Arco, A. Badmaev, C. Wang, C.W. Zhou, 2, 4, 6-Trinitrotoluene (TNT) chemical sensing based on aligned single-walled carbon nanotubes and ZnO nanowires, Adv. Mater. 22 (2010) 1900–1904.
[3] Y.Q. Liang, Z.D. Cui, S.L. Zhu, Z.Y. Li, X.J. Yang, Y.J. Chen, J.M. Ma, Design of a highly sensitive ethanol sensor using a nano-coaxial $p$-$Co_3O_4$/$n$-$TiO_2$ heterojunction synthesized at low temperature, Nanoscale 5 (2013) 10916–10926.
[4] S.M. Majhi, P. Rai, Y.T. Yu, Facile approach to synthesize Au@ ZnO core-shell nanoparticles and their application for highly sensitive and selective gas sensors, ACS Appl. Mater. Interfaces 7 (18) (2015) 9462–9468.
[5] L.L. Li, Y. Chu, Y. Liu, L.H. Dong, Template-free synthesis and photocatalytic properties of novel $Fe_2O_3$ hollow spheres, J. Phys. Chem. C 111 (5) (2007) 2123–2127.
[6] L.S. Zhang, J.S. Hu, H.P. Liang, A.M. Cao, W.G. Song, L.J. Wan, Self-assembled 3D flowerlike iron oxide nanostructures and their application in water treatment, Adv. Mater. 18 (18) (2006) 2426–2431.
[7] J. Chen, L. Xu, W.Y. Li, $\alpha$-$Fe_2O_3$ nanotubes in gas sensor and lithium-ion battery applications, Adv. Mater. 17 (5) (2005) 582–586.

[8] L. Sun, X. Han, K. Liu, S. Yin, Q. Chen, Q. Kuang, Template-free construction of hollow $\alpha$-$Fe_2O_3$ hexagonal nanocolumn particles with an exposed special surface for advanced gas sensing properties, Nanoscale 7 (21) (2015) 9416–9420.
[9] S.G. Chou, P.E. Stutman, S. Wang, E.J. Garoczi, W.F. Egelhoff, D.F. Plusquellic, High-resolution terahertz optical absorption study of the antiferromagnetic resonance transition in hematite ($\alpha$-$Fe_2O_3$), J. Phys. Chem. 116 (30) (2012) 16161–16166.
[10] A. Manikandan, J.J. Vijaya, L.J. Kennedy, Structural optical and magnetic properties of porous $\alpha$-$Fe_2O_3$ nanostructures prepared by rapid combustion method, J. Nanosci. Nanotechnol. 13 (4) (2013) 2986–2992.
[11] G.K. Pradhan, D.K. Padhi, K.M. Parida, Fabrication of $\alpha$-$Fe_2O_3$ Nanorod/RGO composite: a novel hybrid photocatalyst for phenol degradation, ACS Appl. Mater. Interfaces 5 (18) (2013) 9101–9110.
[12] X.C. Jiang, A.B. Yang, Y. Ding, C. Xu, S. Lam, Synthesis and growth of hematite nanodiscs through a facile hydrothermal approach, J. Nanopart. Res. 12 (2010) 877–893.
[13] X. Qu, N. Kobayashi, T. Komatsu, Solid nanotubes comprising $\alpha$-$Fe_2O_3$ nanoparticles prepared from ferritin protein, ACS Nano 4 (3) (2010) 1732–1738.
[14] L. Li, Y. Yu, F. Meng, Y. Tan, R.J. Hamers, S. Jin, Facile solution synthesis of $\alpha$-$FeF_3$. $3H_2O$ nanowires and their conversion to $\alpha$-$Fe_2O_3$ nanowires for photoelectrochemical application, Nano Lett. 12 (2) (2012) 724–731.
[15] H. Quan, B. Cheng, Y. Xiao, S. Lei, One-pot synthesis of a-$Fe_2O_3$ nanoplates-reduced graphene oxide composites for supercapacitor application, Chem. Eng. J. 286 (2016) 165–173.
[16] L.L. Wang, Z. Lou, J. Deng, R. Zhang, T. Zhang, Ethanol gas detection using a yolk-shell (core-shell) $a$-$Fe_2O_3$ nanospheres as sensing material, ACS Appl. Mater. Interfaces 7 (23 2015) 13098–13104.
[17] Y. Wang, J.L. Cao, M.G. Yu, G. Sun, X.D. Wang, H. Bala, Z.Y. Zhang, Porous $a$-$Fe_2O_3$ hollow microspheres: hydrothermal synthesis and their application in ethanol sensors, Mater. Lett. 100 (2013) 102–105.
[18] X. Shang, Z. Guo, W. Gan, R. Zhou, C. Ma, K. Hu, H. Niu, Dye-sensitized solar cells with 3D flower-like $a$-$Fe_2O_3$-decorated reduced graphenes oxide as photoanodes, Ionics 22 (3) (2016) 435–443.
[19] G. Shi, K. Zhang, S. Zhou, Q. Zhang, Template-free synthesis and gas-sensing properties of hierarchical $a$-$Fe_2O_3$ hollow urchin-like spheres, Mater. Lett. 107 (2013) 228–230.
[20] H.N. Zhang, Y.Z. Luo, M. Zhou, T. Yang, J.J. Liang, M. Zhang, J.M. Ma, H.G. Duan, Q.H. Li, Diethylamine gas sensor using $V_2O_5$-decorated $a$-$Fe_2O_3$ nanorods as a sensing material, RSC Adv. 6 (8) (2016) 6511–6515.
[21] P. Gunawan, L. Mei, J. Teo, J. Ma, J. Highfield, Q. Li, Z. Zhong, Ultrahigh sensitivity of Au/1 d $a$-$Fe_2O_3$ to acetone and the sensing mechanism, Langmuir 28 (39) (2012) 14090–14099.
[22] B.Y. Xu, D.L. Zheng, W.W. Qiu, F. Gao, S.X. Jiang, Q.X. Wang, An ultrasensitive DNA biosensor based on covalent immobilization of probe DNA on fern leaf-like $a$-$Fe_2O_3$ and chitosan Hybrid film using terephthalaldehyde as arm-linker, Biosens. Bioelectron. 72 (2015) 175–181.
[23] Y. Zeng, T. Zhang, L.J. Wang, X. Wang, M.H. Kang, H.T. Fan, R. Wang, Y. He, Enhanced toluene sensing characteristics of $TiO_2$-doped flowerlike ZnO nanostructures, Sens. Actuators B 140 (1) (2009) 73–78.
[24] X.M. Xu, X. Li, W.B. Wang, B. Wang, P. Sun, Y.F. Sun, G.Y. Lu, $In_2O_3$ nanoplates: preparation characterization and gas sensing properties, RSC Adv. 4 (10) (2014) 4831–4835.
[25] X.Q. Fu, J.Y. Liu, Y.T. Wan, X.M. Zhang, F.L. Meng, J.H. Liu, Preparation of a leaf-like CdS micro-/nanostructure and its enhanced gas-sensing properties for detecting volatile organic compounds, J. Mater. Chem. 22 (2012) 17782–17791.
[26] J. Yue, X.C. Jiang, A.B. Yu, Molecular dynamics study on metal-deposited iron oxide nanostructures and their gas adsorption behavior, J. Phys. Chem. C 116 (14) (2012) 8145–8153.
[27] J. Chen, L. Xu, W. Li, X, Gou, a-$Fe_2O_3$ nanotubes in gas sensor and lithium-ion battery applications, Adv. Mater. 17 (5) (2005) 582–586.
[28] H. Gong, J.Q. Hu, J.H. Wang, C.H. Ong, F.R. Zhu, Nano-crystalline Cu-doped ZnO thin film gas sensor for CO, Sens. Actuators: B. Chem. 115 (1) (2006) 247–251.
[29] N. Barsan, D. Koziej, U. Weimar, Metal oxide-based gas sensor research: how to? Sens. Actuators B 121 (1) (2007) 18–35.
[30] G. Korotcenkov, Gas response control through structural and chemical modification of metal oxide films: state of the art and approaches, Sens. Actuators B 107 (1) (2005) 209–232.
[31] Y.V. Kaneti, Q.M.D. Zakaria, Z.J. Zhang, C.Y. Chen, J. Yue, M.S. Liu, X.C. Jiang, A.B. Yu, Solvothermal synthesis of ZnO-decorated $a$-$Fe_2O_3$ nanorods with highly enhanced gas-sensing performance toward n-butanol, J. Mater. Chem. A 2 (2014) 13283–13292.
[32] Y.V. Kaneti, J. Moriceau, M.S. Liu, Y. Yuan, Q. Zakaria, X.C. Jiang, A.B. Yu, Hydrothermal synthesis of ternary $a$-$Fe_2O_3$-ZnO-Au nanocomposites with high gas-sensing performance, Sens. Actuators B 209 (2015) 889–897.
[33] X.H. Liu, J. Zhang, X.Z. Guo, S.H. Wu, S.R. Wang, Enhanced sensor response of Ni-doped $SnO_2$ hollow spheres, Sens. Actuators B 152 (2) (2011) 162–167.
[34] H.J. Zhang, R.F. Wu, Z.W. Chen, G. Liu, Z.N. Zhang, Z. Jiao, Self-assembly fabrication of 3D flower-like ZnO hierarchical nanostru-ctures and their gas sensing properties, CrystEngComm 14 (5) (2012) 1775–1782.
[35] J.F. McAleer, P.T. Moseley, J.O.W. Norris, D.E. Williams, Tin dioxide gas sensors. Part 1.-Aspects of the surface chemistry revealed by electrical conductance variations, J. Chem. Soc. Faraday Trans. 83 (4) (1987) 1323–1346.
[36] C. Wang, L. Yin, L. Zhang, D. Xiang, R. Gao, Metal oxide gas sensors: sensitivity and influencing factors, Sensors 10 (3) (2010) 2088–2106.
[37] S.R. Wang, J.D. Yang, H.X. Zhang, Y.S. Wang, X.L. Gao, L.W. Wang, Z.Y. Zhu, One-pot synthesis of 3D hierarchical $SnO_2$ nanostructures and their application for gas sensor, Sens. Actuators B 207 (2015) 83–89.

## Biographies

**Hong Pan** received her B.E. from Southwest University in 2014. She is graduate student in materials science and engineering at Southwest Jiaotong University under the guidance of Professor Weiqing Yang.

**Long Jin** received his B.E. from Southwest Jiaotong University in 2015. He is a graduate student in materials science and engineering at Southwest Jiaotong University under the guidance of Professor Weiqing Yang. His research focuses on the triboelectric nanogenerator.

**Binbin Zhang** was born in March, 1994. He received his B.E. from Southwest Jiaotong University in 2015. He is currently pursuing a doctor's degree in the school of materials science and engineering at Southwest Jiaotong University under the guidance of Professor Weiqing Yang.

**Hai Su** received his Bachelor degree at Chengdu University of Information Technology in 2015 and now his is a master in Prof. Weiqing Yang's group in the Southwest Jiaotong University. His current research interests include flexible and all-solid-state supercapacitors, electrophoretic deposition, electrospinning and micro-supercapacitors etc.

**Haitao Zhang** received his works in PhD in Institute of Electrical Engineering from Chinese Academy of Sciences in 2011. Now he joined School of Materials Science and Engineering, Southwest Jiaotong University as a teacher (assistant professor).

**Weiqing Yang** received his M. S. in Physics in 2007, and PhD in Materials and Science Engineering from Sichuan University in 2011. He was a post-doctorate research fellow at University of Electronic Science and Technology of China from 2011 to 2013. Subsequently, he was a post-doctorate research fellow at Georgia Institute of Technology from 2013 to 2014, under the supervision of Prof. Zhonglin Wang. Now he joined Southwest Jiaotong University as a professor. His current research focuses on nano energy materials, micro-nano devices, and optoelectronic devices.